An Adaptive and Efficient Equalizer Based on Bidirectional Flyback Conversion

Yue Wang, Shiquan Liu, Hankun Liu, Xiangjun Li, *Senior Member, IEEE*, Qi Zhang, *Member, IEEE*, and Yunlong Shang, *Member, IEEE*

***Abstract*—Equalizers are used to improve battery pack consistency and extend battery life, which has been widely applied in the field of electric vehicles and energy storage. However, the traditional equalizers exhibit drawbacks such as large size, low efficiency, and a single equalization function. Therefore, an adaptive and efficient equalization topology based on a bidirectional flyback transform is proposed. The single winding flyback converter bidirectional excitation mechanism is introduced, and only one converter is needed for the whole circuit, realizing low cost and high efficiency equalization. Using odd–even cell grouping control to drive bidirectional excitation, both cell-to-pack and pack-to-cell equalization paths are achieved. Furthermore, three modes, including charging, discharging, and automatic equalization, are supported, making it possible to flexibly choose the suitable equalization approach to achieve fast equalization. Finally, a battery pack experimental platform was built. The results showed that the average equalization efficiency is more than 95%. The voltage difference of the batteries is less than 5 mV after equalization, significantly improving the consistency of the pack. Compared with conventional equalizers, the proposed equalizer is more compact, flexible, and efficient.**

***Index Terms*—Battery, equalizer, excitation, flyback converter.**

I. Introduction

ACHIEVING a clean, low-carbon, and sustainable supply of energy is becoming more urgent as the global demand for energy increases [1]. Lithium-ion batteries possess high energy density, low self-discharge rate, and long cycle life. Consequently, it is widely utilized across several domains [2], [3], [4]. However, lithium-ion batteries are often subject to small differences in voltage or capacity because of differences in production tolerances, usage environments, and charging or discharging conditions [5], [6], [7], [8]. As the battery charge or discharge cycle continues, the differences will be further magnified. Some batteries will age or fail prematurely, which may even cause safety problems such as overheating and fire [9], [10], [11]. Therefore, equalization is indispensable when the lithium-ion battery is in use.

In fact, equalizers are desired to be characterized by low cost, small size, low loss, high speed, and high flexibility. Cost and volume will always be prioritized, whether in electric vehicles (EVs) or energy storage systems (ESSs). Especially in space-constrained EVs, small-size equalizers can help increase the energy density of the battery pack and thus improve range. At the same time, loss and speed must be taken into account, which will affect the energy utilization of the battery pack and the timeliness of the power supply. In addition, facing the inconsistent random distribution of single cells, a highly flexible equalizer also contributes to the speed and efficiency of equalization. In short, the design of compact, efficient, and functionally flexible equalizers is essential and has been widely researched.

After many years of research by scholars, battery equalization technologies have been divided into two types: passive equalization and active equalization [12], [13], [14], [15]. The core of the passive equalization method is consuming excess energy in the battery pack. Specifically, it achieves equalization by consuming the energy of a single cell in the form of heat through resistance. Active equalization attains balance by moving energy from higher voltage cells to lower voltage cells inside the battery pack via a more intricate circuit design. This method adjusts the energy efficiently by using electronic components. Compared with passive equalization, active equalization markedly enhances the energy utilization efficiency of the battery system, avoiding energy waste. At the same time, it reduces the generation of heat, which helps to improve the service life and safety of the battery pack.

Depending on the energy conversion devices, active equalization is divided into capacitively coupled [16], [17], [18], [19], inductively coupled [20], [21], [22], [23], and transformer-based [24], [25], [26], [27], [28], [29]. Meanwhile, active equalization is categorized as voltage-based equalization and state-of-charge (SOC)-based equalization, depending on several equalization algorithms. Among them, the SOC-based method is difficult to estimate with large computational errors, whereas voltage-based equalization only needs to monitor the battery voltage. Due to easy realization, low cost, and easy maintenance voltage-based methods are widely used.

Received 25 January 2025; revised 6 May 2025; accepted 24 June 2025. Date of publication 30 June 2025; date of current version 5 August 2025. This work was supported in part by Shandong Provincial Major Scientific and Technological Innovation Project, China under Grant 2024CXGC010307 and in part by the National Natural Science Foundation of China under Grant 62173211, Grant U24A20159, and Grant 62333013. Recommended for publication by Associate Editor M. Ferdowsi. *(Yue Wang and Shiquan Liu contributed equally to this work.) (Corresponding author: Yunlong Shang.)*

Yue Wang, Shiquan Liu, Hankun Liu, Qi Zhang, and Yunlong Shang are with the School of Control Science and Engineering, Shandong University, Jinan 250061, China (e-mail: moonwang@mail.sdu.edu.cn; 202234100@mail.sdu.edu.cn; 202435014@mail.sdu.edu.cn; zhangqi2013@sdu.edu.cn; yshang@sdu.edu.cn).

Xiangjun Li is with Energy Storage and Electro-Technics Department, China Electric Power Research Institute, Beijing 100192, China (e-mail: lixiangjun@epri.sgcc.com.cn).

Color versions of one or more figures in this article are available at https://doi.org/10.1109/TPEL.2025.3584180.

Digital Object Identifier 10.1109/TPEL.2025.3584180

The basic principle of capacitive active equalization is to store and release electrical energy through a capacitor. The power is regulated by switching devices between the cells. It is suitable for low-power application scenarios. Alvarez-Diazcomas et al. [16] proposed a high-efficiency capacitor-based battery equalizer. This equalizer completely disconnects the capacitor from the circuit at the end of an equalization cycle, solving the inefficiency problem caused by over-equalization. However, the energy can be transferred only between neighboring cells. Meanwhile, a large number of capacitors are required, resulting in a large size and high cost. For this reason, La and Choi [17] proposed a direct cell-to-cell equalizer using a switching matrix, which requires only one capacitor reducing the cost of the circuit and energy loss. Moreover, the energy can be transferred directly between the cells, which greatly shortens the energy flow path. However, the energy storage of capacitors is limited. It can only transfer a small amount of power in a single pass, which is not suitable for large-scale power imbalances. It can be seen that the capacitive active equalization is simple to design and easy to understand. However, the equalization current is small and less flexible.

The basic principle of inductive active equalization is to transfer energy between batteries through inductors and switching devices, which usually provide a larger equalization current compared to capacitive equalization. Liu et al. [20] proposed a dual-layer inductor active equalization topology that mitigates the drawback of an extended energy flow channel. The equalization speed is enhanced by 15.6% relative to the single-layer inductive equalization architecture. However, this equalization circuit necessitates several inductors, resulting in large circuit dimensions and intricate control mechanisms. Guo et al. [21] proposed a single inductor equalization topology. The entire equalization circuit uses only one inductor to transfer energy, which reduces the size of the circuit. However, a large number of MOSFETs and diodes are required, resulting in high cost and complex control. It is worth mentioning that capacitive and inductive equalization are difficult to achieve global equalization (such as cell-to-pack, pack-to-cell) and therefore less flexible.

Unlike the above two methods, the transformer-based method converts and transmits energy by the electromagnetic induction principle, which is more flexible. At the same time, the transformer has natural isolation properties with superior electrical performance. Currently, the transformer-based equalization method is primarily categorized as multitransformer, multiwinding transformer, and a single-winding transformer. Liu et al. [24] proposed a layered parallel equalizer based on a flyback transformer. The equalizer uses hierarchical and parallel equalization techniques to process multiple targets simultaneously, which enhances the efficiency and speed of the equalization process. However, the system with n cells needs $n/2$ flyback converters, which are large and costly. Therefore, Li et al. [25] introduced a hybrid equalization method with a three-winding transformer, which reduces the circuit size and cost. However, it is complex to design multiwinding transformers. Yu et al. [26] proposed an any-cell-to-any-cell equalizer based on flyback conversion. Fig. 1 shows the circuit structure. It allows equalization from any cell to any cell, thus shortening the energy flow path. In comparison with the traditional circuit, the equalization speed is greatly improved. However, the equalization circuit has an obvious drawback. n cells require $4n+4$ switching devices, resulting in a significant increase in circuit cost. More importantly, the reliability of the circuit declines with an increasing number of switching devices.

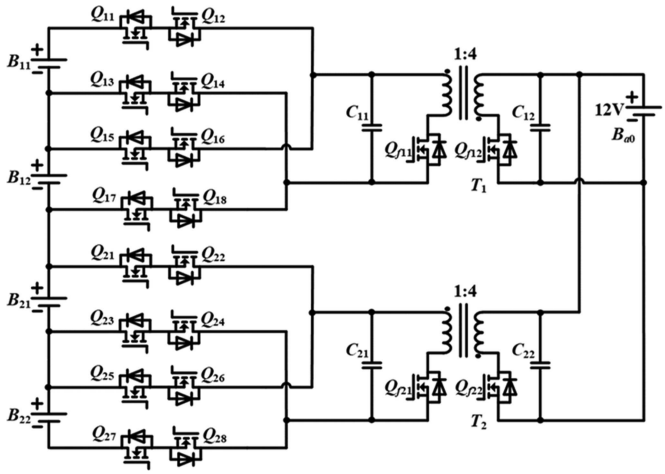

Fig. 1. Any-cell-to-any-cell equalizer based on flyback conversion.

In summary, it is still a challenge to design compact, efficient, and highly flexible equalizers. Motivated by this, an adaptive and efficient equalizer based on a bidirectional flyback transform is proposed in this article. Overall, there are three major contributions of the proposed equalizer. First, the innovative introduction of a single-winding flyback converter bidirectional excitation mechanism in the equalizer. The whole circuit requires only one converter, realizing low-cost and high-efficiency equalization. Second, driving bidirectional excitation based on the odd–even cell grouping control, the equalization paths of any cell-to-pack and pack-to-any cell are simultaneously realized on one converter. Furthermore, three modes of charging, discharging, and automatic equalization, are proposed to provide the equalizer with the ability to adaptively select equalization modes, achieving fast and flexible equalization. Third, the accurate electrical model of the proposed equalizer is established, revealing the influence laws of circuit and control parameters on the performance of the equalizer, which provides theoretical guidance for the design of equalization strategy and optimization of the equalizer. In addition, switching devices have been reduced by about half by sharing switch arrays, further contributing to low cost, small size, and high reliability equalization.

II. Proposed Equalizer

Fig. 2 shows the topology structure of the proposed equalizer containing n cells. The green part on the left side is a switch array for turning ON or OFF the corresponding cell. A monitoring circuit is also included to capture and monitor the cell voltage. The central control unit is used to adjust the pulsewidth modulation (PWM) to control the MOSFETs turn ON or OFF. It can be seen from the topology that the number of flyback transformers will not increase with the scale of the battery pack.

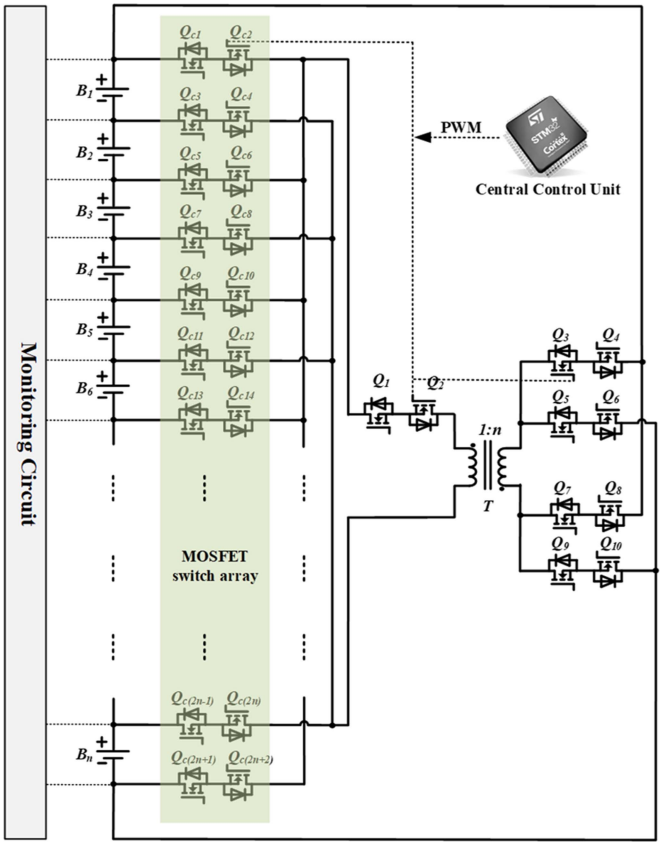

Fig. 2. Proposed equalization topology based on the bidirectional flyback converter.

When the number of cells increases, it is sufficient to add a pair of switches in reverse series in the corresponding branch. In particular, for an n-cell topology, only $2n$+12 MOSFETs and a flyback converter T are required to implement the charging equalization and discharging equalization functions.

The following assumptions are established to better illustrate the working process:

1) The side of the transformer connecting the cell is the primary side. The side connected to the battery pack is the secondary side.
2) On the primary side, the direction of current flow from the cell is positive. On the secondary side, the current flows into the battery pack in a positive direction.
3) The direction of the electromotive force on the primary side is positive when it is "positive up and negative down." The direction of the electromotive force on the secondary side is negative when it is "positive down and negative up."
4) The magnetic flux is positive when the current flows from top to bottom on the primary side. The magnetic flux is negative when the current flows from bottom to top on the secondary side.
5) The positive level of the PWM signal PWM+ controls the MOSFET ON and PWM- controls the MOSFET OFF.
6) Cells B_1, B_3, B_5, …, $B_{(2n-1)}$ are odd cells. Batteries B_2, B_4, B_6, …, $B_{(2n)}$ are even numbered cells.

In circuit operation, there are two processes: single-cell discharging and single-cell charging. These two processes are analyzed below using two cells as an example. It should be emphasized that since many bidirectional switches are used, the state of each switch must be precisely controlled to avoid commutation problems. In addition, only one cell in the battery string exchanges energy during a switching cycle period. If it is desired to change the cell being equalized, it must wait until the last switching cycle has been completed.

A. Discharging Process

Odd and even cells are controlled differently during the discharge process. Fig. 3(a) and (b) shows the discharge process of cell B_1, whereas Fig. 4(a) and (b) shows the discharge process of cell B_2. The energy flows from single cells to the battery pack during the discharge process. The difference is that the magnetic flux is positive when the odd-numbered cells are discharged. The magnetic flux is negative when the even-numbered cells are discharged. The charging and discharging process of neighboring cells realizes the bidirectional excitation of the transformer core. The discharging process of odd and even cells is essentially the same, only the switching array conduction and shutdown are different. Fig. 5(a) shows the key waveform when B_1 is discharging. The frequencies of both PWM1 and PWM2 are f, and the duty cycles are D_1, 1- D_1, respectively. V_{L1} and V_{L2} are the voltages at the primary and secondary sides of the transformer, respectively. i_1 and i_2 are the currents flowing through the primary and secondary sides, respectively. The following is an example of cell B_1 being discharged. There are three operating states in a switching cycle.

State I (t_0 - t_1): Switches Q_{C1}, Q_{C2}, Q_{C3}, Q_{C4}, Q_1, and Q_2 remain ON. All remaining switches remain OFF.

As shown in Fig. 3(a), PWM1 controls the switches to conduct on the primary side of the transformer. PWM2 disables the switches on the secondary side. From t_0, cell B_1 is connected to the circuit. At this point, cell B_1 begins to charge the inductor coil. The magnetic flux increases positively. A positive electromotive force is generated on the primary side, whereas a negative electromotive force is generated on the secondary side. Since the secondary side is turned OFF, there are no current flows. On the primary side, the voltage across the inductor coil V_{L1} can be expressed as

$$V_{L1} = L_P \cdot \frac{di_1}{dt} \tag{1}$$

where L_p is the excitation inductance at the primary side. i_1 is the current at the primary side.

On the primary side, it can be derived from Kirchhoff's law that

$$L_P \frac{di_1}{dt} + i_1 R_p = V_{B1} \tag{2}$$

where V_{B1} is the voltage at the ends of cell B_1. R_p is the equivalent resistance at the primary side. It is a first-order linear nonsingular equation, which is solved to obtain

$$i_1(t) = \frac{V_{B1}}{R_P} \cdot \left(1 - e^{-\frac{R_P}{L_P} \cdot t}\right). \tag{3}$$

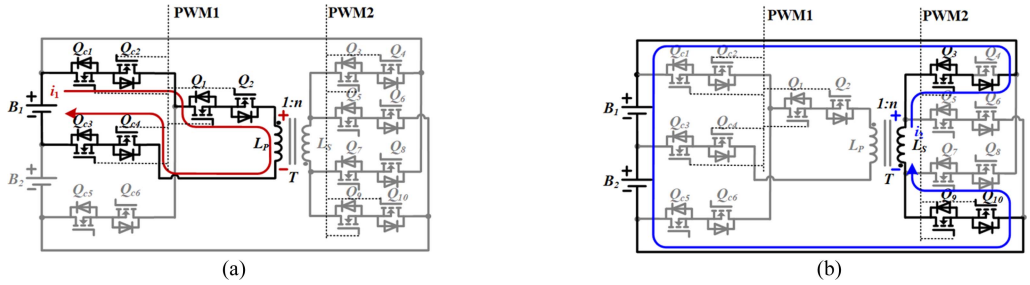

Fig. 3. Cell B1 discharging equivalent circuit diagram. (a) State I. (b) State II.

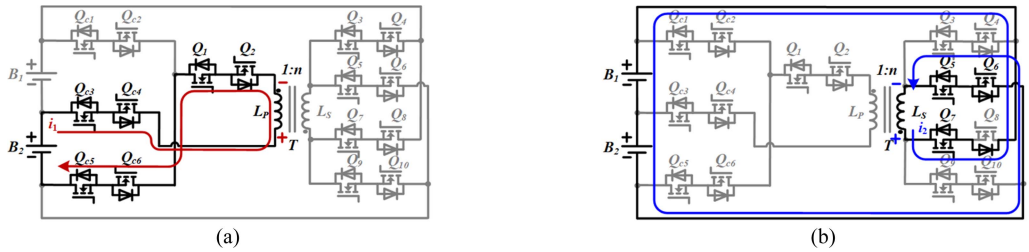

Fig. 4. Cell B2 discharging equivalent circuit diagram. (a) State I. (b) State II.

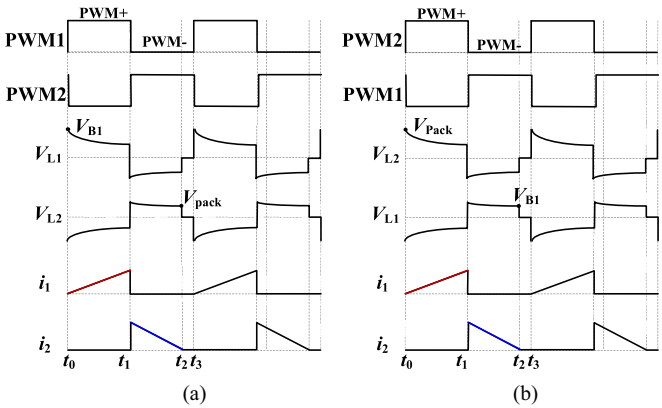

Fig. 5. Key waveforms of voltage and current. (a) During discharging. (b) During charging.

Substituting (3) into (1) gives

$$V_{L1}(t) = V_{B1} \cdot e^{-\frac{R_P}{L_P} \cdot t}. \tag{4}$$

It can be seen from (3) and (4) that i_1 gradually increases from zero. The voltage V_{L1} at the ends coil decreases gradually from V_{B1}. The related waveform is shown in Fig. 5(a) as t_0-t_1.

State II (t_1 - t_2): Switches Q_3, Q_9, and Q_{10} remain ON. All remaining switches remain OFF.

As shown in Fig. 3(b), PWM2 controls the switches to conduct on the secondary side of the transformer. The battery pack is connected to the secondary side. At the moment t_1, a positive electric potential is generated at the secondary side according to the law of electromagnetic induction. At this point, the current on the primary side is renewed through the secondary side. The current flows from the transformer inductor coil to the battery pack. It is worth mentioning that switch Q_4 on the secondary side has to be kept OFF during this process. The current is continued through the body diode of Q_4. When the current drops from the maximum value to zero, Q_4 can effectively prevent the battery pack from recharging the transformer in the reverse direction. The voltage across the inductor coil on the secondary side V_{L2} can be expressed as

$$V_{L2} = -L_S \cdot \frac{di_2}{dt} \tag{5}$$

where L_S is the excitation inductance on the secondary side. i_2 is the current on the secondary side.

On the secondary side, it can be obtained according to Kirchhoff's law

$$-L_S \cdot \frac{di_2}{dt} = i_2 \cdot R_S + V_{\text{Pack}} \tag{6}$$

where V_{Pack} is the voltage across the battery pack. R_S is the equivalent resistance on the secondary side. It is a first-order linear nonsingular equation, which is solved

$$i_2(t) = \left(i_S + \frac{V_{\text{Pack}}}{R_S}\right) \cdot e^{-\frac{R_S}{L_S} \cdot t} - \frac{V_{\text{Pack}}}{R_S} \tag{7}$$

where i_S is the initial current refracted from the primary side to the secondary side. From (7), i_2 gradually decreases from the maximum value i_S and decreases to zero after Δt.

$$\begin{cases} i_S = \frac{1}{n} \cdot \frac{V_{B1}}{R_P} \cdot \left(1 - e^{-\frac{R_P}{L_P \cdot f} \cdot D_1}\right) \\ \Delta t = \frac{L_S}{R_S} \times \ln\left(1 + \frac{R_S \cdot i_S}{V_{\text{Pack}}}\right) \end{cases} \tag{8}$$

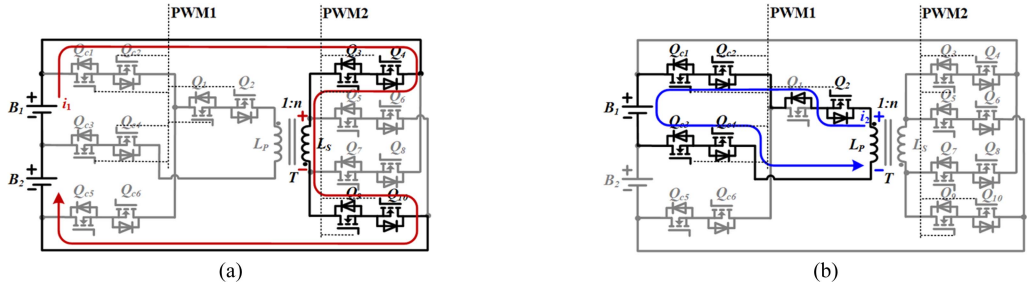

Fig. 6. Cell B1 charging equivalent circuit diagram. (a) State I. (b) State II.

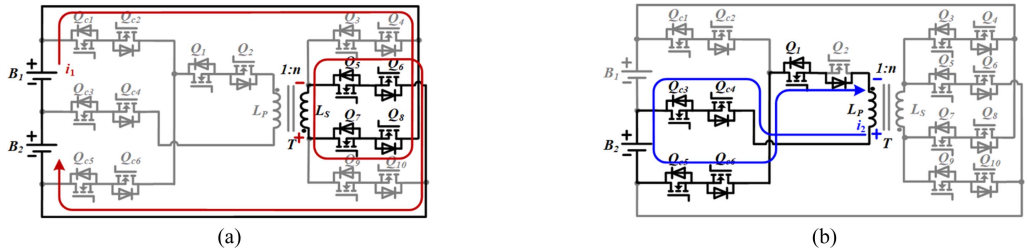

Fig. 7. Cell B2 charging equivalent circuit diagram. (a) State I. (b) State II.

where n is the winding turns ratio. Substituting (7) into (5) gives

$$V_{L2}(t) = (R_S \cdot i_S + V_{\text{Pack}}) \cdot e^{-\frac{R_S}{L_S} \cdot t}. \tag{9}$$

From (9), the voltage V_{L2} at the ends of the transformer coil gradually decreases from its maximum value. After Δt, V_{L2} decreases to V_{Pack}. At this point, B_1 stops discharging. The transformer is completely demagnetized. The relevant waveform is shown in the t_1-t_2 segment in Fig. 5(a).

State III (t_2 - t_3): Switches Q_3, Q_9, and Q_{10} remain ON. All the remaining switches remain OFF.

In this stage, the switches are in the same state as in the previous stage. Since Q_4 always remains OFF, the current can only be renewed through the Q_4 body diode. In other words, the current flows only from the transformer to the battery pack. Therefore, the equalizer is naturally in the static state when the current on the secondary side of the transformer drops to zero. During an equalization cycle, it is necessary to rationally allocate the ON–OFF times of the primary and secondary sides. Ensure that the secondary side conduction time (t_3-t_1) is greater than Δt in (8) as

$$t_3 - t_1 = \frac{1-D_1}{f} > \frac{L_S}{R_S} \cdot \ln \times \left(1 + \frac{R_S \cdot \frac{1}{n} \cdot \frac{V_{B1}}{R_P} \cdot \left(1 - e^{-\frac{R_P}{L_P \cdot f} \cdot D_1} \right)}{V_{\text{Pack}}} \right). \tag{10}$$

It can be ensured that the circuit operates in the discontinuous conduction mode (DCM) intermittent state. The transformer is fully demagnetized after one equalization cycle.

B. Charging Process

Odd and even cells are controlled differently during the charge process. Fig. 6(a) and (b) shows the charge process of cell B_1. Fig. 7(a) and (b) shows the charging process of cell B_2. The energy is transferred from the battery pack to the single cell during the charging process. The difference is that the magnetic flux is positive when the odd-numbered cells are charged. The magnetic flux is negative when the even-numbered cells are charged. The charging processes of odd and even cells are essentially the same, only the switching array conduction and shutdown are different. Fig. 5(b) shows the key waveform when B_1 is charged. The following is an example of cell B_1 being charged. There are three operating states in a switching cycle.

State I (t_0 - t_1): Switches Q_3, Q_4, Q_9, and Q_{10} remain ON. All the remaining switches remain OFF.

As shown in Fig. 6(a), PWM2 controls the switches to conduct on the secondary side of the transformer. PWM1 controls the switches to turn OFF on the primary side. From t_0, the battery pack connects to the circuit, at which time the battery pack charges the inductor coil. The magnetic flux increases positively. The secondary side generates a positive electromotive force while the primary side generates a negative electromotive force. Since the primary side is turned OFF, no current flows. Similar to the battery discharge process, according to Kirchhoff's law, the formula of current i_1 variation on the secondary side can be obtained

$$i_1(t) = \frac{V_{\text{Pack}}}{R_S} \cdot \left(1 - e^{-\frac{R_S}{L_S} \cdot t} \right) \tag{11}$$

where V_{Pack} is the battery pack terminal voltage. R_{S} is the transformer secondary sideline equivalent resistance. L_{S} is the excitation inductance on the secondary side.

The secondary side inductor coil terminal voltage V_{L2} is

$$V_{L2}(t) = V_{\mathrm{Pack}} \cdot e^{-\frac{R_S}{L_S} \cdot t}. \tag{12}$$

From (11) and (12), i_1 gradually increases from zero. The voltage V_{L2} at the ends coil gradually decreases from V_{Pack}. The related waveforms are shown as t_0-t_1 in Fig. 5(b).

State II (t_1 - t_2): Switches Q_{C1}, Q_{C2}, Q_{C3}, Q_{C4}, and Q_2 remain ON. All the remaining switches remain OFF.

As shown in Fig. 6(b), PWM1 controls the switches to conduct on the primary side of the transformer. Cell B_1 is connected to the primary side. At the moment t_1, according to the law of electromagnetic induction, a positive electric potential is generated at the primary side. At this time, the current in the secondary side is renewed through the primary side. The current flows from the inductive coil of the transformer to cell B_1. It is worth mentioning that the Switch Q_1 on the primary side has to be kept OFF during this process. The current is renewed through the body diode of Q_1. When the current drops from the maximum value to zero, Q_1 can effectively prevent cell B_1 from recharging the transformer in the reverse direction.

According to Kirchhoff's law, the changing current i_2 on the primary side can be obtained as

$$i_2(t) = \left(i_P + \frac{V_{B1}}{R_P}\right) \cdot e^{-\frac{R_P}{L_P} \cdot t} - \frac{V_{B1}}{R_P} \tag{13}$$

where V_{B1} is the voltage across cell B_1. R_{P} is the equivalent resistance at the primary side. L_{P} is the excitation inductance at the primary side. i_{P} is the initial current refracted from the secondary side to the primary side.

From (13), i_2 gradually decreases from the maximum value i_{P} to zero after Δt as

$$t_2 - t_1 = \Delta t = \frac{L_P}{R_P} \cdot \ln\left(1 + \frac{R_P \cdot i_P}{V_{B1}}\right). \tag{14}$$

The primary side inductor coil terminal voltage V_{L1} is

$$V_{L1}(t) = (R_P \cdot i_P + V_{B1}) \cdot e^{-\frac{R_P}{L_P} \cdot t}. \tag{15}$$

From (15), the voltage V_{L1} at the ends of the transformer coil gradually decreases from its maximum value. After Δt, V_{L1} decreases to V_{B1}. At this point, the charging process is stopped. The transformer is completely demagnetized. The relevant waveform is shown in the t_1-t_2 segment in Fig. 5(b).

State III (t_2 - t_3): Switches Q_{C1}, Q_{C2}, Q_{C3}, Q_{C4}, and Q_2 remain ON. All the remaining switches remain OFF.

In this stage, the status of the switches is consistent with the previous stage. Since Q_1 always remains OFF, the current can only be renewed through the Q_1 body diode. In other words, the current can only flow from the transformer to cell B_1. Therefore, the equalizer will be in a static state when the current on the primary side drops to zero. During one equalization cycle, it is necessary to reasonably allocate the ON–OFF times on the primary and secondary sides so that the conductive time t_3-t_1 on the primary side is greater than Δt in (14). The timing conditions are analyzed similarly to (10). This ensures that the circuit operates in the DCM intermittent state. The transformer can be completely demagnetized after one equalization cycle. Combining the analysis of the discharging process, the equalizer operates in DCM mode in both processes. This results in a periodic reset of the magnetic flux, which is not only effective in avoiding core saturation, but also avoids flux imbalance and reduces hysteresis losses.

In addition, it is easy to notice that despite the reduction of about half of the switches on the primary side compared to the topology proposed in Fig. 1, the same number of switches are used between the battery cells and the transformer during the charging and discharging process (ignoring Q_1 and Q_2 shared by the battery pack). This not only realizes the same energy flow, but also avoids the stress increase that may be caused by the switch reduction.

C. Efficiency Analysis

To reasonably evaluate the performance of the equalizer, the equalization efficiency can be described by the energy of the battery pack before and after equalization. The conventional approach considers a single cell as a large capacitor with constant capacitance whose energy can be calculated by $0.5CV^2$, and the efficiency can be given as [32]

$$\eta = \frac{\sum_{i=1}^{n} \frac{1}{2} \cdot C \cdot V_{\mathrm{end},i}^2}{\sum_{i=1}^{n} \frac{1}{2} \cdot C \cdot V_{\mathrm{start},i}^2} \cdot 100\% = \frac{\sum_{i=1}^{n} V_{\mathrm{end},i}^2}{\sum_{i=1}^{n} V_{\mathrm{start},i}^2} \cdot 100\% \tag{16}$$

where i and C are the single cell number and equivalent capacitance, respectively. $V_{\mathrm{start},i}$ and $V_{\mathrm{end},i}$ are the voltages of cell i at the beginning and end of equalization, respectively. However, it assumes a linear relationship between battery voltage and stored charge, which is usually at odds with reality. To improve the calculation method, a nonlinear model of the capacitance–voltage (C–V) relationship is required.

The energy E stored in a single cell can also be expressed as

$$E = Q \cdot V = \frac{SOC}{100} \cdot Q_r \cdot V \tag{17}$$

where Q, SOC, V, and Q_r are the current charge, state of charge, voltage, and battery rated charge/discharge capacity. The unit of Q and Q_r is Ah. Obviously, E should be equal to the energy calculated using the equivalent capacitance value, which in turn can be derived as

$$C = \frac{SOC}{V} \cdot \frac{2 \cdot 3600 \cdot Q_r}{100} = 72 \cdot \frac{F(V) \cdot Q_r}{V} \tag{18}$$

where $F(V)$ is the mapping from voltage to SOC, which can be obtained by a lookup table based on charge/discharge test data. It should be noted that $F(V)$ and Q_r are different under charging and discharging conditions due to battery characteristics. For charging and discharging, $F(V)$ is represented by $F_{\mathrm{chr}}(V)$ and $F_{\mathrm{dis}}(V)$, and Q_r is represented by Q_{chr} and Q_{dis}, respectively. According to the actual average charging and discharging currents of the equalization topology, the battery was tested to obtain $F_{\mathrm{chr}}(V)$ and $F_{\mathrm{dis}}(V)$, and Q_{chr} and Q_{dis} were measured to be 30.981

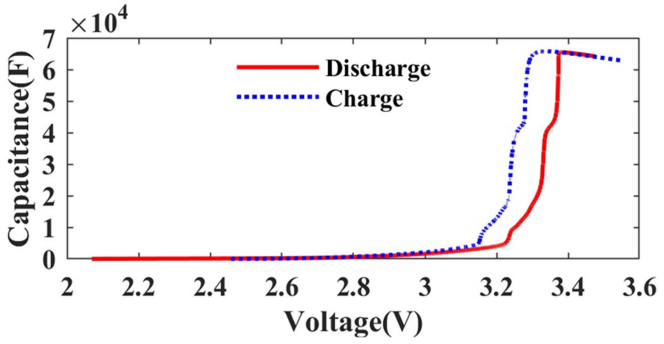

Fig. 8. *C–V* relationship based on battery test.

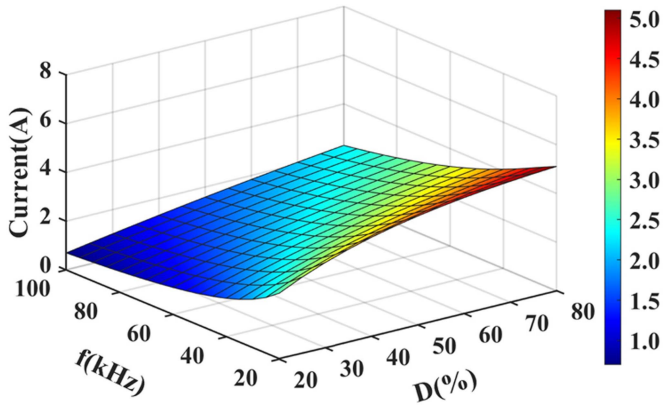

Fig. 9. Variation of the equalization current with switching frequency *f* and duty cycle *D*.

and 30.967 Ah, respectively. Based on the test data, the *C–V* relationship is obtained, as shown in Fig. 8.

Furthermore, according to the capacitive energy calculation formula mentioned in (16), the energy at the beginning of equalization of each battery can be expressed as

$$E_{\text{start},i}=36\cdot F_c(V_{\text{start},i})\cdot V_{\text{start},i}\cdot Q_c,\ c=\begin{cases}dis, V_{\text{start},i}\geq V_{\text{end},i}\\ chr, V_{\text{start},i}<V_{\text{end},i}\end{cases} \tag{19}$$

where c is the charging and discharging conditions. To simplify the analysis, it is determined whether it is a charging process or a discharging process according to the beginning and ending voltages..

Similarly, the energy at the end of equalization for each cell can be expressed as

$$E_{\text{end},i}=36\cdot F_c(V_{\text{end},i})\cdot V_{\text{end},i}\cdot Q_c,\ c=\begin{cases}\text{dis}, V_{\text{start},i}\geq V_{\text{end},i}\\ \text{chr}, V_{\text{start},i}<V_{\text{end},i}\end{cases}. \tag{20}$$

Finally, the efficiency can be calculated as

$$\eta=\frac{E_{\text{end}}}{E_{\text{start}}}\cdot 100\%=\frac{\sum_{i=1}^{n}E_{\text{end},i}}{\sum_{i=1}^{n}E_{\text{start},i}}\cdot 100\%. \tag{21}$$

III. Design Rules for Equalizer

The design of the equalizer consists of two main parts: transformer design and equalization strategy design.

A. Flyback Converter Design

During the design of the transformer, parameters such as switching frequency f, duty cycle D, primary side inductance L_{P}, secondary side inductance L_{S}, and coil turns ratio n need to be determined.

1) Switching Frequency f *and Duty Cycle* D*:* Fig. 9 shows the variation of the equalization current with switching frequency f and duty cycle D when the cell is discharged. The equalization current will become larger as the inductor charging time increases. Therefore, the equalization speed can be accelerated by decreasing the switching frequency f and increasing the duty cycle D of the on-time. However, the decrease in the switching frequency will cause the size of the transformer to rise. Meanwhile, the circuit losses will increase as the switching frequency increases. The switching frequency of the circuit needs to be set in a reasonable range. Usually, the switching frequency of the flyback converter is set between 20–100 kHz. Considering the equalization current and DCM timing conditions, the discharging equalization frequency is set to 25 kHz with a duty cycle of 50%. The charging equalization frequency is set to 50 kHz with a duty cycle of 30%.

2) Winding Inductance L *and Turns Ratio* n*.:* According to (3), the smaller the winding inductance L, the higher the equalization current. Theoretically, the winding inductance can be reduced infinitely to raise the equalization speed. However, the winding inductance value of the transformer is not infinitely reducible as the energy conversion device in the equalization process. As the inductance value decreases, the energy stored in the transformer will gradually decrease during an equalization cycle. Eventually, the current will reach saturation status in the process of increasing. Through Simulink and Maxwell joint simulation, the inductance L_{P} on the primary side of the transformer is set to about 8 μH according to the equalization frequency f determined in 1). The transformer turns ratio n is set to 1:4. At this time, the equalization current reaches about 4 A.

In transformer design, a ferrite core is used, whose low coercivity and low remanent magnetization not only help to reduce hysteresis losses, but also help to ensure the symmetry of the *B–H* loop. The core needs to be open-air gapped to prevent transformer saturation. Also, the inductance is usually controlled by changing the core air gap length. A large air gap length will result in a rapid increase in leakage flux, leading to an increase in coil eddy current losses. Conversely, a small air gap length will lead to higher machining accuracy requirements, which is not favorable for transformer fabrication. According to design experience, the core air gap length is usually set between 0.1 and 1.5 mm. Table I gives the relevant parameters of the designed transformer T. $L_{\text{P/S}}$ is the excitation inductance on the primary and secondary sides. L_{eq} is the leakage inductance. R_{eq} is the equivalent resistance of the transformer coil. N_{p} and N_{s} are the number of turns on the primary and secondary sides. It is worth mentioning that leakage inductance is unavoidable in flyback

TABLE I
TRANSFORMER PARAMETERS

Parameter	Transformer T	
	P	S
$L_{P/S}$ (μH)	8.02	113.75
L_{eq} (μH)	0.22	3.62
R_{eq} (Ω)	0.016	0.135
N_p	3	
N_s	12	

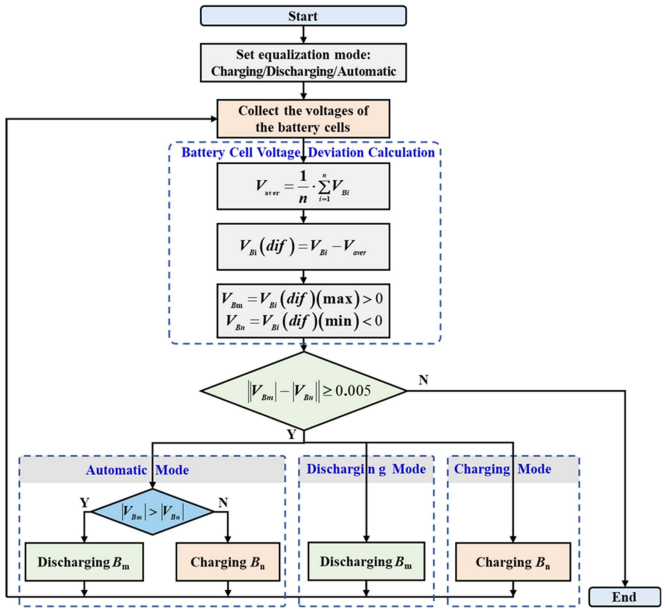

Fig. 10. Equalization strategy flowchart.

converters, which leads to voltage spikes, efficiency losses, and electromagnetic interference. Fortunately, with proper design, the maximum leakage inductance of a flyback converter is only about 3%, which not only reduces turn-OFF losses but also effectively reduces the spike voltage. At the same time, both sides of the transformer consist of a number of series switches to withstand the spike voltage, leaving ample design margins. Therefore, it is permissible not to use buffers or clamping circuits in this design. However, adding them is beneficial for circuit reliability and lifetime.

B. Equalization Strategy Design

To improve the flexibility of equalization, three equalization modes are designed according to the characteristics of the proposed equalizer: discharging equalization, charging equalization, and automatic equalization. Fig. 10 shows the equalization strategy flowchart. For battery packs with different voltage distributions, the most suitable equalization mode can be selected accordingly to complete the equalization with the fastest speed. A detailed description of the equalization process is given as follows:

1) Setting the equalization mode, which is temporarily selected manually in this article. Manufacturers can also integrate algorithms to automatically select the equalization mode after the voltage is acquired in the next step.
2) Collect and record the voltage of each single cell, as V_{Bi} ($i = 1,2,3,\ \ldots, n$).
3) Calculate the average voltage of all cells, denoted as V_{aver}.

$$V_{\mathrm{aver}} = \frac{1}{n}\cdot\sum_{i=1}^{n} V_{\mathrm{Bi}}. \tag{22}$$

4) Calculate the difference between each single cell and the average voltage, denoted as $V_{\mathrm{Bi}}(dif)$.

$$V_{\mathrm{Bi}}(dif) = V_{\mathrm{Bi}} - V_{\mathrm{aver}}. \tag{23}$$

5) Record the first maximum value in V_{Bi}(dif) as V_{Bm}. Record the first minimum value in V_{Bi}(dif) as V_{Bn}. Obviously, $V_{\mathrm{Bm}}>0$ and $V_{\mathrm{Bn}}<0$. The corresponding cells are recorded as B_{m} and B_{n}, respectively.
6) Discharging equalization: continuously discharge B_{m}.

Charging equalization: Continuously charge B_{n}.
Automatic equalization: If $|V_{\mathrm{Bm}}|>|V_{\mathrm{Bn}}|$, perform a period of discharging process for B_{m}. Otherwise, perform a period of charging process for B_{n}.

1) Repeat (2)–(6). Until the difference between $|V_{\mathrm{Bm}}|$ and $|V_{\mathrm{Bn}}|$ is less than the set threshold (typically 5 mV).

It can be seen that in the discharging equalization mode, the equalizer always selects the highest voltage battery to discharge until the maximum voltage difference is below the set threshold. This applies to situations when a few cells have significantly high voltages. In charging equalization mode, the equalizer is continuously charging the lowest voltage battery until the maximum voltage difference is below the set threshold. This applies to situations when a few cells have significantly low voltages. In automatic equalization mode, battery charging and discharging are alternated. This applies when the voltage is evenly distributed. In summary, it is possible to flexibly choose the suitable equalization approach according to different voltage distributions to achieve fast equalization. In fact, it can be further combined with numerical analysis, machine learning, and other algorithms to automatically identify the voltage distribution after each round of voltage acquisition, and then provide a more theoretically supported equalization mode selection.

In conclusion, the proposed equalizer focuses on the energy transfer path at the hardware level and the voltage extreme values at the software level. It means that as long as the characteristics of the battery pack do not affect the topological energy transfer and the acquisition of voltage extreme values, it is theoretically applicable to the proposed equalizer.

IV. EXPERIMENTAL RESULTS

Based on the topology principle, a balanced experimental prototype supporting 12 batteries was designed. Fig. 11 shows the experimental platform, including the center control unit

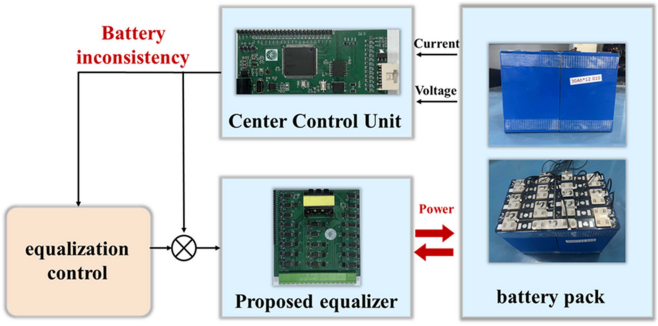

Fig. 11. Experimental prototype with 12 series-connected batteries.

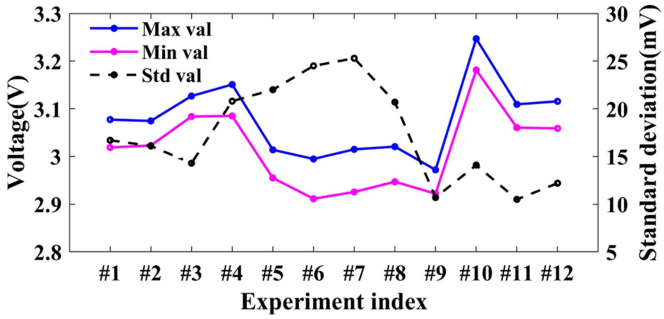

Fig. 12. Initial voltage distribution for all experiments.

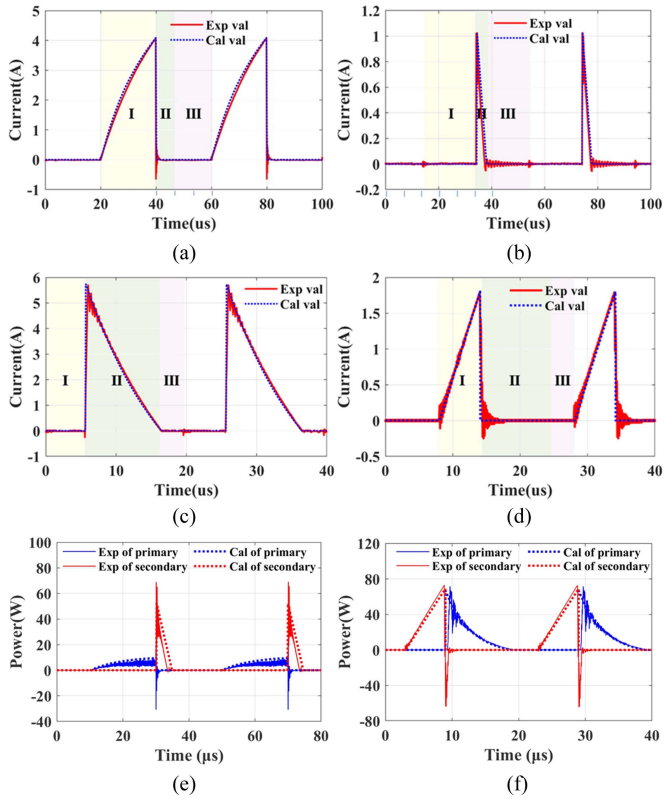

Fig. 13. Experimental curves of the transformer. (a) Current of the primary side during discharging. (b) Current of the secondary side during discharging. (c) Current of the primary side during charging. (d) Current of the secondary side during charging. (e) Power flow waveform of the transformer during discharging. (f) Power flow waveform of the transformer during charging.

board (with a size of 10 cm × 5 cm), the equalizer board (with a size of 10 cm × 10 cm), and the battery pack. The center control unit is core to the STM32F103ZET6 microcontroller unit and is programmed in C within the KEIL integrated environment. It integrates the voltage collection module driver, the PWM output module, and the equalization judgment logic shown in Fig. 10. The analog front-end chip XL8812 is selected as the core of the voltage collection module, which has a maximum error of no more than 2 mV for single cell voltage acquisition in the actual hardware, and can provide reliable data support for the equalization action. Combining the collected voltages, the center control unit outputs PWM to the proposed equalizer based on the equalization strategy, which in turn drives the corresponding MOSFETs ON or OFF. The part number of the MOSFET is WSP08N15, which is inexpensive, and the rated V_{DS}, I_d, and $R_{DS(ON)}$ are 50 V, 8 A, and 60 mΩ, respectively, leaving enough margin for equalization current and spike voltage.

The battery pack consists of 12 lithium-iron-phosphate batteries with a capacity of 30 Ah connected in series. To verify the effectiveness of the equalization circuit, 12 groups of equalization experiments, numbered from #1 to #12, were conducted. In particular, #1 to #4 are discharging equalization, #5 to #8 are charging equalization, and #9 to #12 are automatic equalization. The initial voltage distribution for all experiments is shown in Fig. 12.

A. Discharging Equalization

During the battery discharging process, the equalization frequency is set to 25 kHz. The duty cycle of conduction time is set to 50% for both the primary and secondary sides of the transformer. The equivalent resistance R_P is measured to be 0.55 Ω on the primary side. According to (3), the equalization current i_1 is about 4 A. Fig. 13(a) and (b) shows the current changes on the transformer during the equalization process. It can be seen that the experimental results are consistent with the theoretical calculations. Fig. 13(e) shows the experimental and simulated values of power flow on both sides of the transformer. It can be seen that the maximum power on the primary and secondary sides is about 10 W and 50 W, respectively, and the experimental values match the simulated values. However, it can be observed that at the moment corresponding to t_1 in Fig. 5(a), the experimental value shows a significant power peak, which is caused by the spike voltage generated by the leakage inductance when the primary side switches are closed. Based on the power flow, the primary side power is integrated for t_0 to t_1 in Fig. 5(a) as the input energy, and the secondary side power is integrated for the t_1 to t_3 as the output energy, and the efficiency of the converter can be calculated to be 98.8%.

Fig. 14(a) and (c) shows the initial voltage distribution of the pack for experiments #1 and #2, as well as the trend of the voltage change. It is observed that the voltages gradually converge. According to the statistics of Fig. 14(b) and (d), the maximum voltage differential and standard deviation of experiment #1 were reduced from 60 mV and 16.7 mV to 5 mV

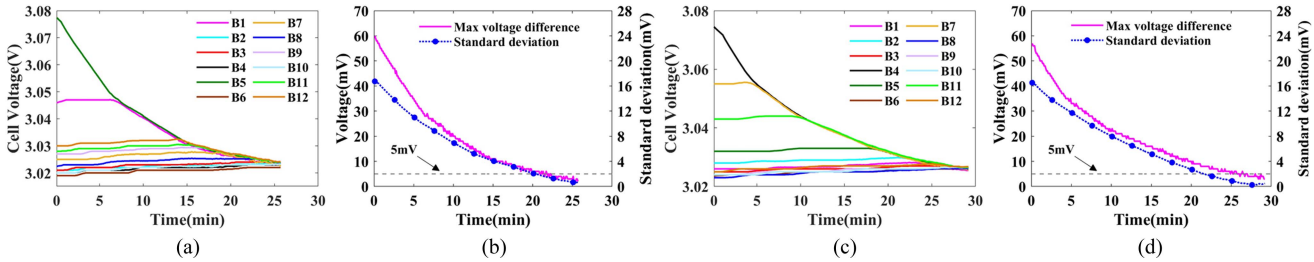

Fig. 14. Results of the discharging equalization experiment. (a) Voltage curves of experiment #1. (b) Consistency statistics of experiment #1. (c) Voltage curves of experiment #2. (d) Consistency statistics of experiment #2.

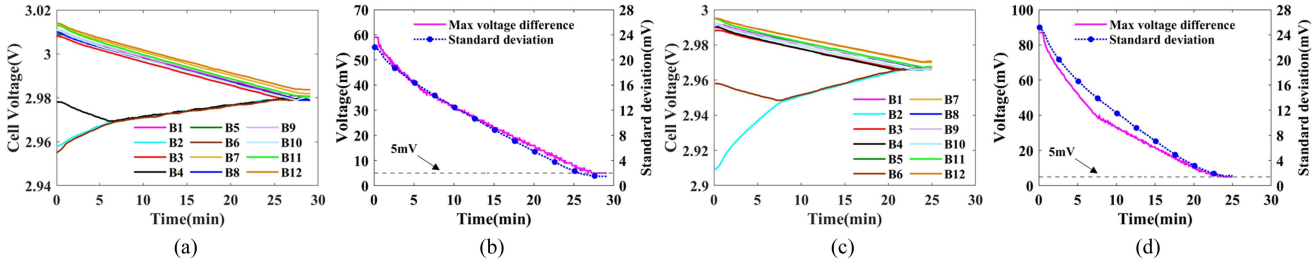

Fig. 15. Results of charging equalization experiment. (a) Voltage curves of experiment #5. (b) Consistency statistics of experiment #5. (c) Voltage curves of experiment #6. (d) Consistency statistics of experiment #6.

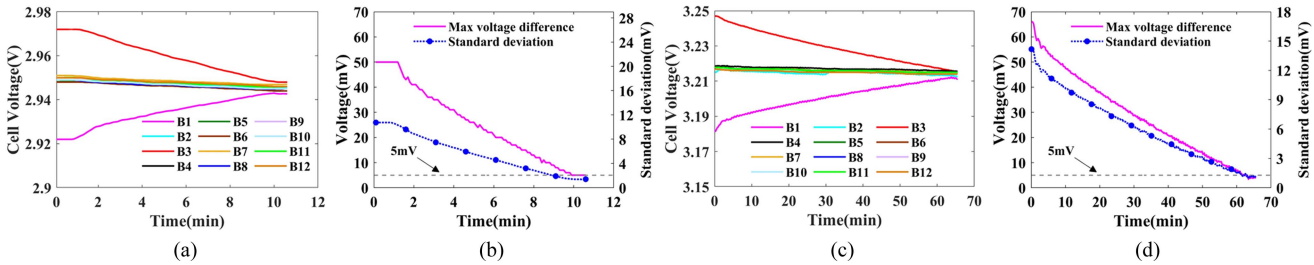

Fig. 16. Results of the automatic equalization experiment. (a) Voltage curves of experiment #9. (b) Consistency statistics of experiment #9. (c) Voltage curves of experiment #10. (d) Consistency statistics of experiment #10.

and 2.1 mV, respectively, and those of experiment #2 from 57 mV and 16.5 mV to 5 mV and 0.9 mV, respectively.

B. Charging Equalization

During battery charging, the equalization frequency is set to 50 kHz. The duty cycle is set to 70% of the conduction time on the primary side. The secondary side on-time duty cycle is set to 30%. The equivalent resistance R_S on the secondary side is measured to be 2.51 Ω. According to (13), the equalization current i_2 is about 6 A. Fig. 13(c) and (d) shows the current changes on the primary and secondary sides during the equalization process. It can be seen that the experimental results are compatible with the theoretical calculations. As can be observed from the power flow in Fig. 13(f), the maximum power on both primary and secondary sides is about 70 W, and the experimental value matches the simulation value. It is also observed that the spike voltage generated by the leakage inductance leads to the power peak on the secondary side. Similar to the converter efficiency analysis process for the discharging process, the converter efficiency during charging was calculated to be 87.6%.

Similarly, it can be seen from Fig. 15(a) and (c) that the voltages converged gradually. According to the statistics of Fig. 15(b) and (d), the maximum voltage differential and standard deviation of experiment #5 were reduced from 59 mV and 22 mV to 5 mV and 1.6 mV, respectively, and those of experiment #6 from 87 mV and 25.2 mV to 5 mV and 1.5 mV, respectively.

C. Automatic Equalization

In automatic equalization mode, the single cells are alternately charged and discharged. The parameters of the circuit were the same as the discharge and charging equalization. Fig. 16 shows the initial voltage distribution of the pack and the voltage trends for experiments #9 and #10. It can also be seen that the voltages gradually converge. The maximum voltage differential and standard deviation of experiment #9 were reduced from 50 mV and 10.7 mV to 5 mV and 1.4 mV, respectively, and

TABLE II
COMPARISON OF SEVERAL EXISTING EQUALIZERS

Equalizers	Components						Equalization current	Circuit cost	Circuit size	Control complexity	Equalization speed	Equalization efficiency
	SW	D	L	C	T	W						
Capacitor [16]	$2n$	0	0	n - 1	0	0	0.1A	Low	High	Low	Slow	91.68%
Inductor [21]	$2n+2$	$2n$	1	0	0	0	0.6A	Medium	Low	High	Slow	93.26%
Multitransformer equalizer [24]	$3n$	0	0	0	$n/2$	1	2.4A	High	High	High	Medium	98.80%
Multi-winding equalizer [25]	$2n+5$	$2n+4$	0	0	1	3	1.5A	Medium	Medium	High	Medium	95.0%
Single winding equalizer [26]	$4n+4$	0	0	0	2	1	2.4A	High	High	High	Medium	/
Proposed equalizer	$2n+10$	0	0	0	1	1	5.8A	Low	Low	Medium	Fast	98.70%

n is the number of cells in the battery pack. SW: MOSFET switches. D: Diode. L: Inductors. C: Capacitors. T: Transformers. W: Windings in one transformer.

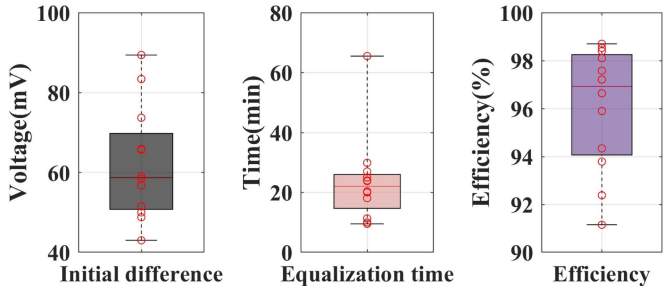

Fig. 17. Experimental results statistics.

those of experiment #10 from 66 mV and 14.2 mV to 5 mV and 1.3 mV, respectively.

Finally, Fig. 17 shows the statistical results of all the experiments, including the initial voltage difference, the equalization time, and the equalization efficiency. It can be seen that the initial voltage differences are mainly concentrated between 50 and 70 mV, with maximum and minimum values of 89.4 mV and 43 mV, respectively. The equalization times are mainly concentrated between 15 and 27 min, with maximum and minimum values of 65.5 and 9.5 min, respectively. The efficiencies are mainly concentrated between 94% and 98.4%, with maximum and minimum values of 98.7% and 91.15%, respectively. On average, the proposed equalizer can reduce the battery pack voltage difference by 57.1 mV in 23.7 min, with an efficiency of 96.06%.

It is worth noting that for larger initial imbalances as well as for aged battery packs, they do not affect either the topological energy transfer or the acquisition of voltage extreme values. Therefore, they are also applicable to the proposed equalizer, although these scenarios may result in an increase in the equalization time or the number of equalization actions.

V. COMPARISON WITH EXISTING EQUALIZERS

Table II presents a comparison of various existing equalizers with the proposed equalizer. The comparison items include the number of devices used, equalization current, circuit cost, circuit volume, control complexity, equalization efficiency, etc. All the comparisons are for n-cell batteries. In particular, the equalization current is adjustable in various equalization circuits. Theoretically, it can reach any value needed. To better match the engineering reality, the equalization current in Table II is the maximum operating current of the equalizer designed in the experiments.

The capacitor-based equalization circuits generally have the obvious disadvantage of a small equalization current. The current of the equalizer designed in [16] is only 100 mA. At the same time, the circuit requires a large number of capacitors for energy exchange. It has the disadvantage of a large circuit size and slow equalization speed. The inductor-based equalization circuit proposed in [21] requires plenty of switches and has a small equalization current. There are problems with complex circuit control and slow equalization speed. Different from the capacitor and inductor-based equalizer, the transformer-based equalizer has a large current and fast equalization speed. More importantly, the equalization efficiency usually exceeds 95%. However, this type of equalizer requires a large number of MOSFETs, leading to elevated circuit costs and intricate control mechanisms. In the multitransformer-based equalization circuit proposed in [24], the number of transformers increases with the scale of the battery pack. Inevitably, the circuit volume is large. In the multiwinding transformer-based equalizer proposed in [25], only one transformer is required for the entire circuit. The circuit size is moderate. However, the design of the multiwinding transformer is complex. There are magnetic coupling and interference problems between different windings. In the single winding equalization circuit proposed in [26], as many as $4n+4$ switches are required for n cells, resulting in a sudden increase in the cost. More importantly, the reliability decreases subsequently.

Compared with the various equalizers in the past, the proposed equalizer has been optimized in many aspects. First, the circuit cost is greatly reduced. The MOSFETs are reduced by about 50% compared to [26]. In addition, the entire equalization circuit requires only a single-winding transformer. The volume and weight of the topology are markedly diminished. Second, benefiting from the rational design of the flyback converter, the proposed equalizer provides an efficiency of up to 98.7% with an average of 96.6%. Third, the equalizer also has multiple equalization modes, which can flexibly adapt to different equalization scenarios. Finally, the peak current of the designed equalizer is

up to 5.8 A, resulting in a fast equalization speed. It can be seen that the proposed equalizer provides the best performance when the equalization current ratio cost or volume is used as a comparison metric. In short, the proposed equalizer is compact, fast, efficient, and flexible.

It is worth mentioning that high equalization currents may conflict with battery degradation, thermal management issues, electromagnetic compatibility issues, and cost increases. But the proposed equalizer provides a higher upper current limit, giving a wider optimization space for comprehensive optimization. In conclusion, the proposed equalizer has outstanding performance in terms of circuit size, cost efficiency, etc.

VI. Conclusion

In this article, an adaptive and efficient equalizer based on a bidirectional flyback transform is proposed. First, the topology configuration of the equalizer is described in detail. Then, the working principles of the proposed equalizer are analyzed. Based on this, the equalization experimental platform is built. The experimental results not only verify the correctness of the theoretical analysis but also show that the equalizer has the following superior performance:

1) The proposed equalizer enables both cell-to-pack and pack-to-cell equalization paths.
2) By optimizing the circuit structure, the proposed equalizer is compact, has low cost, and is simple to control.
3) The entire equalization system requires only a single-winding flyback converter by bidirectional excitation of the transformer core. It achieves more than 95% equalization efficiency on average at a lower cost.
4) The equalizer exists in various working modes. It can flexibly adapt to different equalization scenarios to complete fast equalization. On average, it can reduce the maximum differential voltage of the battery pack by 58 mV in 21 min.

Although the proposed topology provides multiple equalization modes for adaptive equalization, how to automatically determine the equalization modes based on voltage distribution remains to be studied. In the future, the voltage distribution identification algorithm based on machine learning will be researched to realize the automatic selection of equalization modes. In addition, a snubber or clamp circuit is planned to be included to improve the reliability of the circuit.

References

[1] Z. G. Yang, J. L. Zhang, K.-M. Michael, and X. C. Lu, "Electrochemical energy storage for green grid," *Chem. Rev.*, vol. 111, no. 5, pp. 3577–3613, Jun. 2011.

[2] H. Liu, Y. Wang, T. Wang, Y. Gong, and Y. Shang, "A dual-stage thermal runaway early warning strategy for lithium-ion batteries based on multi-domain acoustic signal fusion," *Energy*, vol. 322, May 2025, Art. no. 135748.

[3] A. Pamidimukkala, S. Kermanshachi, J. M. Rosenberger, and G. Hladik, "Barriers and motivators to the adoption of electric vehicles: A global review," *Green Energy Intell. Transp.*, vol. 3, no. 2, 2024, Art. no. 100153.

[4] Y. Shang, N. Cui, B. Duan, and C. Zhang, "Analysis and optimization of star-structured switched-capacitor equalizers for series-connected battery strings," *IEEE Trans. Power Electron.*, vol. 33, no. 11, pp. 9631–9646, Nov. 2018.

[5] X. Gong, R. Xiong, and C. C. Mi, "Study of the characteristics of battery packs in electric vehicles with parallel-connected lithium-ion battery cells," *IEEE Trans. Ind. Appl.*, vol. 51, no. 2, pp. 1872–1879, Mar./Apr. 2015.

[6] J. Jiao et al., "Layered energy equalization structure for series battery pack based on multiple optimal matching," *Green Energy Intell. Transp.*, vol. 4, no. 2, Apr. 2025, Art. no. 100182.

[7] M. Uno and A. Kukita, "String-to-battery voltage equalizer based on a half-bridge converter with multistacked current doublers for series-connected batteries," *IEEE Trans. Power Electron.*, vol. 34, no. 2, pp. 1286–1298, Feb. 2019.

[8] Y. Wang, Y. Shang, X. Gu, J. Li, and C. Zhang, "An incipient multi-fault diagnosis method for lithium-ion battery pack based on data-driven with incremental-scale," *IEEE Trans. Transp. Electrific.*, vol. 10, no. 4, pp. 9554–9565, Dec. 2024.

[9] C. Hua and Y.-H. Fang, "A charge equalizer with a combination of APWM and PFM control based on a modified half-bridge converter," *IEEE Trans. Power Electron.*, vol. 31, no. 4, pp. 2970–2979, Apr. 2016.

[10] B. Duan, Z. Y. Li, P. W. Gu, Z. K. Zhou, and C. H. Zhang, "Evaluation of battery inconsistency based on information entropy," *J. Energy Storage*, vol. 16, pp. 160–166, Apr. 2018.

[11] Y. J. Zheng, W. K. Gao, and M. G. Ouyang, "State-of-charge inconsistency estimation of lithium-ion battery pack using mean-difference model and extended Kalman filter," *J. Power Sources*, vol. 383, pp. 50–58, Dec. 2018.

[12] H. Zhang, Y. Wang, H. Qi, and J. Zhang, "Active battery equalization method based on redundant battery for electric vehicles," *IEEE Trans. Veh. Technol.*, vol. 68, no. 8, pp. 7531–7543, Aug. 2019.

[13] Y. Chen, X. Liu, Y. Cui, J. Zou, and S. Yang, "A multiwinding transformer cell-to-cell active equalization method for lithium-ion batteries with reduced number of driving circuits," *IEEE Trans. Power Electron.*, vol. 31, no. 7, pp. 4916–4929, Jul. 2016.

[14] X. Qi, M. Fang, Y. Wang, Y. Wang, and Z. Chen, "An equalization current ripple cancellation (ECRC) converter-based centralized equalization system for series-connected battery strings," *IEEE Trans. Transp. Electrific.*, vol. 9, no. 2, pp. 2765–2777, Jun. 2023.

[15] J. Nie, R. Fu, C. Cai, J. Ma, Z. Shu, and L. Ma, "A high efficiency battery equalizing circuit based on half bridge topology with multiport transformer," *IEEE Trans. Ind. Electron.*, vol. 71, no. 3, pp. 2522–2532, Mar. 2024.

[16] A. Alvarez-Diazcomas, A. A. Estevez, and R. Carrillo, "A high-efficiency capacitor-based battery equalizer for electric vehicles," *Sensors*, vol. 23, no. 11, 2023, Art. no. 5009.

[17] P.-H. La and S.-J. Choi, "Direct cell-to-cell equalizer for series battery string using switch-matrix single-capacitor equalizer and optimal pairing algorithm," *IEEE Trans. Power Electron.*, vol. 37, no. 7, pp. 8625–8639, Jul. 2022.

[18] C. Lu, L. Kang, S. Wang, Z. Wang, and H. Rao, "A novel inductor-based non-dissipative equalizer," *Energies*, vol. 11, no. 10, Oct. 2018, Art. no. 2816.

[19] X. Ding et al., "A novel active equalization topology for series-connected lithium-ion battery packs," *IEEE Trans. Ind. Appl.*, vol. 56, no. 6, pp. 6892–6903, Nov./Dec. 2020.

[20] X. Liu, H. Pang, and Y. Geng, "Dual-layer inductor active equalization control for series-connected lithium-ion batteries based on SOC estimation," *Electronics*, vol. 11, no. 8, 2022, Art. no. 1169.

[21] X. Guo, Q. Wu, C. Xing, W. Qian, and Y. Zhao, "An active equalization method for series-parallel battery pack based on an inductor," *J. Energy Storage*, vol. 64, 2023, Art. no. 107157.

[22] Y. Shang, C. Zhang, N. Cui, and C. C. Mi, "A delta-structured switched-capacitor equalizer for series-connected battery strings," *IEEE Trans. Power Electron.*, vol. 34, no. 1, pp. 452–461, Jan. 2019.

[23] Y. Shang, B. Xia, F. Lu, C. Zhang, N. Cui, and C. C. Mi, "A switched-coupling-capacitor equalizer for series-connected battery strings," *IEEE Trans. Power Electron.*, vol. 32, no. 10, pp. 7694–7706, Oct. 2017.

[24] H. Liu, X. Wei, J. Ai, and X. Yang, "A layered parallel equaliser based on flyback transformer multiplexed for lithium-ion battery system," *Energies*, vol. 17, no. 3, 2024, Art. no. 754.

[25] B. Li, X. Wang, X. Zou, Z. Zheng, and S. Li, "Hybrid equalization scheme for a lithium-ion battery pack based on a three-winding transformer," *Int. J. Circuit Theory Appl.*, vol. 52, pp. 3988–4006, Aug. 2024.

[26] K. Yu, Y. Shang, X. Wang, N. Wang, B. Duan, and C. Zhang, "A multi-cell-to-multi-cell equalizer for series-connected batteries based on flyback conversion," in *Proc. 3rd Conf. Veh. Control Intell.*, 2019, pp. 1–5.

[27] Y. Shang, N. Cui, B. Duan, and C. Zhang, "A global modular equalizer based on forward conversion for series-connected battery strings," *IEEE J. Emerg. Sel. Top. Power Electron.*, vol. 6, no. 3, pp. 1456–1469, Sep. 2018.

[28] B. Xu et al., "Modularized equalization architecture with transformer-based integrating voltage equalizer for the series-connected battery pack in electric bicycles," *IEEE Trans. Ind. Electron.*, vol. 70, no. 7, pp. 6984–6992, Jul. 2023.
[29] Y. Shang, B. Xia, C. Zhang, N. Cui, J. Yang, and C. Mi, "A modularization method for battery equalizers using multiwinding transformers," *IEEE Trans. Veh. Technol.*, vol. 66, no. 10, pp. 8710–8722, Oct. 2017.
[30] S. Wang, Y. Wang, G. Chen, D. Wei, and Y. Shang, "An efficient and compact equalizer based on forward-flyback conversion for large-scale energy storage systems," *IEEE Trans. Transp. Electrific.*, vol. 10, no. 1, pp. 1222–1232, Mar. 2024.
[31] S. Liu, Y. Wang, S. Wang, W. Zhao, and Y. Shang, "A compact large-current equalizer based on flyback conversion for large-scale battery packs," *IEEE Trans. Power Electron.*, vol. 40, no. 1, pp. 738–748, Jan. 2025.
[32] Y. Ye and K. W. E. Cheng, "Modeling and analysis of series–parallel switched-capacitor voltage equalizer for battery/supercapacitor strings," *IEEE J. Emerg. Sel. Topics. Power Electron.*, vol. 3, no. 4, pp. 977–983, Dec. 2015.

Yue Wang received the M.E. degree in electrical engineering from Qingdao University, Qingdao, China, in 2019. He is currently working toward the Ph.D. degree in control science and engineering with the School of Control Science and Engineering, Shandong University, Jinan, China.

His research interests include battery safety, efficient utilization, and battery management system design.

Shiquan Liu received the B.S. degree in automation from Qingdao University, Qingdao, China, in 2022. He is currently working toward the M.S. degree in control science and engineering with the School of Control Science and Engineering, Shandong University, Jinan, China.

His research interests include battery balancing and battery charging.

Hankun Liu received the B.S. degree in electrical engineering and automation from Shandong Jianzhu University, Jinan, China, in 2024. She is currently working toward the M.E. degree in electric engineering with the School of Control Science and Engineering, Shandong University, Jinan, China.

Her research interests include battery fault detection and battery safety.

Xiangjun Li (Senior Member, IEEE) received the Ph.D. degree in electrical and electronic engineering from the Kitami Institute of Technology, Kitami, Japan, in 2006.

Since June 2019, he has been the Director at Energy Storage System Integration and Configuration Technology Research Laboratory, Energy Storage and Electro-Technics Department, China Electric Power Research Institute, Beijing, China.

His research interests include the topic of digital intelligence, operation control, and application technologies for energy storage systems, electric vehicles, and microgrids.

Qi Zhang (Member, IEEE) received the B.S. degree in automation and the M.S. degree in control science and engineering, in 2010 and 2013, respectively, from Shandong University, Jinan, China, where he is currently working toward the Ph.D. degree with the School of Control Science and Engineering.

In 2013, he joined Shandong University, where he is currently an Associate Researcher and a Senior Engineer. His research interests include electric vehicles and battery management technology.

Yunlong Shang (Member, IEEE) received the B.S. degree in automation from the Hefei University of Technology, Hefei, China, in 2008, and the Ph.D. degree in control theory and control engineering from Shandong University, Jinan, China, in 2017.

In 2019, he joined Shandong University, where he is currently a Professor with the School of Control Science and Engineering. Between September 2015 and October 2017, he conducted scientific research as a joint Ph.D. student with the Department of Electrical and Computer Engineering, San Diego State University, where, between December 2017 and January 2019, he was a Postdoctoral Research Fellow. His research interests include battery balancing, battery modeling and state estimation, self-heating for low-temperature batteries, and design of battery management systems.

Dr. Shang was the recipient of the Outstanding Paper Award from IEEE TRANSACTIONS ON INDUSTRIAL ELECTRONICS in 2022.